THE JOURNAL OF PHYSICAL CHEMISTRY B

Miami

Subscriber access provided by University Of Miami Libraries

B: Biophysics; Physical Chemistry of Biological Systems and Biomolecules

Investigating Polyoxometalate-Protein Interactions at Chemically Distinct Binding Sites

Thomas J Paul, Tatjana Parac-Vogt, David Quiñonero, and Rajeev Prabhakar

J. Phys. Chem. B, **Just Accepted Manuscript** • DOI: 10.1021/acs.jpcb.8b02931 • Publication Date (Web): 05 Jul 2018

ACS Publications

is published by the American Chemical Society. 1155 Sixteenth Street N.W., Washington, DC 20036

Investigating Polyoxometalate-Protein Interactions at Chemically Distinct Binding Sites

Thomas J. Paul[§], Tatjana N. Parac-Vogt[†], David Quiñonero[‡] and Rajeev Prabhakar[§,*]

§ *Department of Chemistry, University of Miami, Coral Gables, FL 33146*

† *Department of Chemistry, KU Leuven, Leuven, Belgium*

‡ *Department of Chemistry, Universitat de les Illes Balears, Palma de Mallorca, Spain*

[*] To whom correspondence should be addressed; rpr@miami.edu; Tel: 305-284-9372; Fax: 305-284-4571.

Abstract. In this study, a combined molecular docking (rigid and flexible) and all-atom molecular dynamics (MD) simulations technique have been employed to investigate interactions of 1:1 Zr-containing Keggin Polyoxometalate (ZrK) with four chemically distinct cleavage sites [Arg114-Leu115 (site 1), Ala257-Asp258 (site 2), Lys313-Asp314 (site 3), and Cys392-Glu393 (site 4)] of human serum albumin (HSA). The ZrK-HSA complexations were analyzed using electrostatic potentials, chemical nature of amino acid residues, binding free energies, and secondary structures as parameters. They suggested that ZrK binds in a rather distinct manner to different cleavage sites and its association was dominated by hydrogen bonding, both direct and solvent mediated, and electrostatic interactions, as suggested experimentally. The computed binding free interaction energies (-57.5, -24.2, -50.8, and -91.2 kJ/mol for site 1, 2 ,3 and 4, respectively) predicted the existence of one major binding site (site 4) and three minor binding sites (site 1, site 2, and site 3). The strong exothermicity of the binding was also supported by isothermal calorimetry (ITC) experiments. Additionally, the binding of ZrK did not alter the overall α-helical secondary structure of HSA, which was in line with experimental observation. Furthermore, hydrolysis of the peptide bonds of the substrate was found to retain its overall structure. These results have provided a deeper understanding of the complex ZrK interactions with proteins and will lead to the design of the next generation of catalytically active POMs with improved hydrolytic activities.

I. Introduction. Polyoxometalates (POMs) are a versatile class of metal-oxygen clusters that utilize their molecular properties like charge, oxidation state, ligand environment, and photochemical characteristics in diverse fields such as catalysis, materials science, and analytical chemistry.[1-3,4-12] Due to their specificity towards different biomolecules, they also exhibit antiviral[13], antitumoral[14], antibacterial[15], and anticancer activities[16]. Additionally, they have been used in ribosomal crystallography[17] and for the inhibition of HIV reverse transcriptase[18] and HIV protease activity[19]. POMs have also shown to inhibit amyloid beta peptides (Aß)[20] and basic fibroblast growth factor (bBGF)[21]. Furthermore, as a hydrolytic agent, Zr(IV)-substituted POMs (Zr-POMs) have been reported to hydrolyze multiple peptide bonds of critical biomolecules including human serum albumin (HSA),[1, 22] hen egg-white lysozyme (HEWL)[23], myoglobin[1, 24], b-insulin[24] and and cytohrome c[25]. The peptide bond is extremely stable and its half-life is estimated to be between 350-600 years under physiological conditions.[26] However, the hydrolysis of this bond has been involved in a wide range of biotechnological, biomedical, and industrial applications like proteomics[27], protein engineering[28], protein footprinting,[29-32] protein sequencing[33-35], bioethanol production[36], and catalytic drugs[37-38]. Moreover, peptide bond cleaving enzymes constitute about 60% of all enzymes that are used in textile, food, leather, paper, and ethanol production industries.[36] For hydrolytic activities, Zr-POMs are required to coordinate near specific cleavage sites of their substrates such as HSA.[23] This Zr-POM-substrate association has been postulated to be driven by either electrostatic interaction of the negatively charged oxygen atoms of POM with the positively charged regions on the substrate's surface or coordination of the oxophilic Zr(IV) ion to the amino acid side chains in the protein.[39-44] The noncovalent interactions in this process could occur both directly and indirectly through the mediation of solvent molecules.

HSA is one of the most abundant proteins in blood plasma with a concentration of 40 mg/mL.[45] It is considered as one of the major soluble constituents of the circulatory system and contributes significantly to colloid osmotic pressure and transport, and distribution, and metabolism of ligands.[46-48] Fatty acids, amino acids, metal ions, and various hydrophobic and acidic drugs are included in this ligand subset which is responsible for numerous critical processes within the liver, intestine, kidneys, and the brain.[46-48] Due to its biological functions, HSA has been considered one of the best studied models to understand the physicochemical basis of drug-protein interactions.[49]

Recently, hydrolysis of HSA by a variety of POMs $[(nBu_4N)_5[\{W_5O_{18}Zr(\mu\text{-}OH)\}_2].2H_2O$ (Zr2-L2), $(Et_2NH_2)_{10}[Zr(PW_{11}O_{39})_2].7H_2O$ (Zr1-K2), $(Et_2NH_2)_8[\{\alpha\text{-}PW_{11}O_{39}Zr(\mu\text{-}OH)(H_2O)\}_2].7H_2O$ (Zr2-K2), and $K_{15}H$ $[Zr(\alpha_2\text{-}P_2W_{17}O_{61})_2].25H_2O$ (Zr1-WD2)] at pH 7.4 and 60 °C was investigated.[1] The SDS page data indicated that peptide hydrolysis occurred at the same region of HSA in the presence of each POM. After 48 hours, less than 35% of HSA was hydrolyzed by the Zr-containing Keggin POM (Zr1-K2). However, after 192 hours, the extent of hydrolysis was significantly increased.[1] Since this reaction required the coordination of the carbonyl oxygen of the peptide bond of the substrate to the Zr(IV) ion, the dimeric 1:2 Keggin form (Zr1-K2) was unlikely to be the reactive species in the absence of a vacant site on the metal ion. The increased substrate concentration was previously reported to influence the 1:2 POM speciation, shifting the equilibrium towards the monomeric (1:1) species that was capable of the aforementioned coordination.[50-51] Additionally, using Eu(III) luminescence spectroscopy, it was shown that in the presence of HSA the 1:2 (Zr1-K2) complex could convert into the monomeric 1:1 (ZrK) species at physiological pH and low POM concentrations (Figure 1a).[52] Furthermore, monomeric ZrK

was found to be bound to another biomolecule, HEWL, in a co-crystal structure of the ZrK-HEWL complex.[53]

From western blot and subsequent NH_2-terminal Edman degradation analysis, four distinct cleavage sites (Arg114-Leu115, Ala257-Asp258, Lys313-Asp314, and Cys392-Glu393) located in different regions of HSA were identified (Figure 1b).[1] ZrK was quite versatile and unlike most natural proteases, in a rather non-preferential manner, it cleaved a variety of peptide bonds formed by chemically diverse amino acid residues i.e. polar charged (Arg, Asp and Glu) and nonpolar (Leu, Ala and Cys). Cleavage site 1 (Arg114-Leu115) was located in the central cleft of HSA within a positive inner surface. The width of the cleft was reported to be roughly 1 nm in size, which was quite comparable to the size of ZrK. Site 1, as in all sites, was flanked by a positively charged surface patch, which could facilitate interactions with the negatively charged groups of ZrK.[1] The remaining cleavage sites Ala257-Asp258, Lys313-Asp314, and Cys392-Glu393 of HSA occurred upstream from negatively charged Asp or Glu residues suggesting that there could also be a possible electrostatic interaction with the positively charged Zr(IV) or W ions of ZrK. However, the hydrolysis requires coordination of the carbonyl oxygen of the peptide bond to the Zr(IV) ion and from experiments, a weak ionic interaction rather than true coordination was suggested.[1] Interestingly, it appears that charge plays a larger role in binding of ZrPOMs to HSA as an increase in negative charge of the POM metal cluster resulted in increased reactivity, while the addition of more of Zr(IV) ions in its framework showed no apparent change.[1]

In the absence of X-ray structures of the POM-HSA complexes, the physicochemical nature of their interactions at multiple cleavage sites are not known. The understanding of these interactions at the atomistic level is required for utilization of POMs in a variety of biochemical, biotechnological, and medical applications. In this aspect, molecular dynamics (MD) simulations can provide structural information and elucidate the nature of POM-HSA interactions. Recently, this technique was successfully utilized to explore association of HEWL with a variety of Ce(IV) substituted POMs.[44] However, to the best of our knowledge, interactions of a single POM with multiple chemically distinct cleavage sites of a protein have thus far not been investigated. Furthermore, changes in the secondary structure of protein after the binding of POM and its hydrolysis are not known.

In this study, we have employed all-atom MD simulations using ZrK and HSA as models to address all these unresolved issues. The results are compared with the available experimental data. Our simulations will provide structures of ZrK-HSA complexes at all four chemically distinct cleavage sites and elucidate their specificities. They will also help to elucidate roles of dynamics, specific amino acid residues, solvent, charge distributions, secondary structures, and binding affinities in POM-proteins interactions. Furthermore, they will contribute to design the next generation of POMs with enzyme-like activities.

II. Computational Procedure. The structures of ZrK and HSA were obtained from the Protein Data Bank (PDB ID: 4XYY and 4K2C, respectively).[53-54] The X-ray structure of ZrK after including a hydroxyl nucleophile was fully optimized without any geometrical constraint

employing DFT functional B3LYP[55] and Lanl2dz[56] (W and Zr) and 6-31G*[57] (O and H) basis sets as implemented in the Gaussian 09[58] program. The X-ray structure of HSA was relaxed in an explicit aqueous environment for 100 ns utilizing all-atom MD simulations. Molecular docking was performed using Autodock Vina 1.5.6 software[59] to obtain poses of binding of ZrK-HSA complexes around the four cleavage sites that were proposed experimentally.[1] Two molecular docking methods were utilized, rigid docking and flexible docking. The latter provided conformational flexibility to amino acid residues of HSA upon binding of ZrK. The size of the grid was chosen to cover these binding sites, and the spacing was kept to 1.00 Å. Each docking trial produced 20 poses with an exhaustiveness value equal to 20. The most promising poses provided by these docking procedures were subsequently used for MD simulations utilizing the GROMACS program[60-61] and AMBER03[62] force field. It is noteworthy that ZrK and POMs in general are very complex molecules to treat using molecular mechanics. The RESP charges for ZrK were calculated and used to form a topology file using antechamber,[63-64] an in-built tool in Amber.[65] The set of Lennard-Jones parameters for the W and O atoms of the ZrK framework were taken from previous works [66-67] while the parameters for Zr were taken from the UFF force field.[68] The ZrK metal cluster was treated as a semi-rigid body during the simulations where the oxygen and tungsten cage was held together using a matrix, a distance restrains with high energetic penalty (≥ 1000 kJ/mol), for conformational deviations. For all simulations, the starting structures were placed in a cubic box with dimensions of 100 × 100 × 100 Å. This dismisses unwanted effects that may arise from the applied periodic boundary conditions (PBC). The box was filled with TIP3P[69] water molecules. Some water molecules were replaced by sodium and chloride ions to neutralize the system (overall charge = -18) and to simulate a physiological ion concentration of 154 mM. The starting structures were subsequently energy-

minimized with a steepest descent method for 3000 steps freezing binding site coordinates to minimize rearrangement. The results of these minimizations produced the starting structures for the MD simulations. The MD simulations were run for 100 ns each for all four sites. These simulations were performed using a constant number of particles (N), pressure (P), and temperature (T) i.e. NPT ensemble. The SETTLE algorithm[70] was used to constrain the bond lengths and angles of the water molecules, while the LINCS algorithm[71] was used to constrain the bond lengths of the peptide. The long-range electrostatic interactions were calculated by the Particle-Mesh Ewald (PME) method.[72] A constant pressure of 1 bar was applied with a coupling constant of 1.0 ps; peptide, water molecules, and ions were coupled separately to a bath at 300 K with a coupling constant of 0.1 ps. The trajectories were computed for each model with a time step of 2 fs, and the data was saved every 500 steps. The ionizable amino acid residues were set to their normal ionization states at pH 7.0. The tools available in GROMACS were utilized to analyze the MD trajectories. We used the most representative structures for the structural elucidation. The most representative structures were derived from a cluster analysis, where the trajectories are analyzed by grouping structurally similar frames [root-mean-square deviation (rmsd) cutoff of 0.30 nm], while the frame with the largest number of neighbors are denoted as a middle structure that represents that particular cluster. The computed rmsd values confirmed the equilibration of all structures within the simulation timeframe (Figure S1). Noncovalent interaction (NCI) plots were calculated using the NCIPLOT program.[73-74] This program provides an index that is based on electron density and its derivatives that allows for the identification of noncovalent interactions. The binding free energies were calculated using a thermodynamic cycle that describes the bound and unbound states utilizing the lambda (λ) particle approach. Using a thermodynamic cycle, the relative binding energies of two ligands can be described by

the difference in free energy associated with the chemical change of one ligand into the other in the bound and solvated environments.[75] This approach has been described in detail in previous works.[75-77] In these calculations, van der Waals and Coulombic interactions between ZrK and HSA were turned off in a systematic way, first Coulombic terms were diminished followed by the van der Waals terms. This allowed no oppositely-charged atoms to interact at very close distances which would have resulted in unstable configurations and unreliable energies. The efficient leap-frog stochastic dynamics (sd) integrator was used along with the neighbor searching cutoff scheme Verlet with a frequency value of 20.[78-80] Standard compressibility and Parrinello-Rahman[81] pressure coupling was used which is an extended-ensemble coupling where the box vectors are subject to equations of motion every 1.0 ps. The value of the α scaling factor used for the soft-core Lennard-Jones equations was set to 0.5 with a power of 1.0 associated with λ. The σ value, assigned to any atom that has C6 and C12 parameters that equal zero, was 0.3 which is typical for the treatment of hydrogen atoms. Secondary structure diagrams were generated for all complexes studied from productions runs utilizing the inbuilt tools mdmat and DSSP[82-83], respectively within the GROMACS package. Electrostatic surface potentials for HSA were calculated using the Adaptive Poisson-Boltzmann Solver (APBS)[84] software and visualized with PyMol.[85] YASARA[86-87] and Chimera[88] programs were used for visualization and for the preparation of the structural diagrams presented in this study. ONIOM calculations were performed to probe the possibility of negatively charged residues interacting with the positive character originating from the W metals of ZrK. In these calculations, the system was divided into two parts, a selected model system [ZrK (POM), Aps13, and Asp255] where treated with quantum mechanics while the remaining part of HSA was treated with molecular mechanics. The ONIOM optimization procedure used macro/microiterations[89] and the electrostatic interactions

between the QM and the MM regions were treated by mechanical embedding (ME). The geometry was optimized without any symmetrical constraints at the B3LYP/Lanl2dz level of theory[55, 90] [With corresponding Hay-Wadt effective core potential (ECP) for Zr, and W[91]], and the 6-31G(d) basis set was used for all the other atoms in the QM layer. The MM part was treated using the AMBER force field.[92-93]

III. Results and Discussion. In this study, interactions of ZrK with four chemically distinct cleavage sites that are located in different parts of the HSA have been explored using all-atom MD simulations. The structures of all ZrK-HSA complexes and their interactions have been discussed using electrostatic potentials, chemical nature of individual amino acid residues, binding free energies, and secondary structures as parameters.

IIIa. ZrK-HSA interactions at site 1 (Arg114-Leu115). The first cleavage site (Arg114-Leu115, site 1) was formed by a positively charged (Arg) and a nonpolar (Leu) residue. This site was a part of a random coil section on the surface of HSA that showed little to no secondary structure (Figure 2a). The electrostatic potential map (Figure 2b), suggested two positively charged regions on either side of the peptide bond. Thus, both rigid and flexible docking of ZrK around this site provided two possible binding motifs. The first motif included two positive residues Arg114 and Lys137 of HSA that were present on the exterior surface of the cleavage site. The stability of this site was tested through MD simulations. There were no ZrK-HSA interactions at this site throughout the MD trajectory and the overall non-bonding energies were very small. However, during the simulation, ZrK moved down to a more hydrophobic cleft

formed by the Val120-Lys137 region. The second binding motif from the docking procedure was found on the opposite side of site 1. It was located on the interior of the cleavage site, where a large pocket surrounded by many positively charged residues allowed for binding of a negatively charged ZrK. This site, termed FA1, has previously been identified to bind long chain fatty acids.[94] Given the flexible nature of random coil sections, this site was easily accessible for the binding of ZrK. The size of this site was roughly 1.0 nm and could easily accommodate Keggin-type POMs (length ≤1.0 nm), however larger POMs such as Wells-Dawson (length ≥1.2 nm) would not be accommodated as easily. Furthermore, this site was buried within the protein which could further limits larger POMs from entering the binding site. However, the first binding motif suggested by the docking procedure was located on the surface of HSA (roughly 2.0 nm in length) which could easily accommodate the larger Wells-Dawson POMs.

The FA1 site was stabilized by host of hydrogen bonding from positively charged amino acid residues of HSA. These types of interactions have been previously proposed to drive association of POMs with biomolecules.[95-97] For instance, Arg117, Arg186, and Arg428 formed multiple hydrogen bonds through interactions between their amine protons and the negatively charged oxygen cage of ZrK (Figure 2c). Additionally, positively charged Lys190 and Lys519 residues associated through hydrogen bonding with the surface of ZrK (Figure 2c and d). The negatively charged surface of ZrK preferred positive patches along the protein surface and readily bound to these sections even in the presence of negatively charged residues (Asp/Glu). These residues should in theory repel the ZrK from binding however; here this repulsion was overcome by greater attractive hydrogen bonding and electrostatic interactions originating from positively charged residues (Figure S4). The geometrical constraints imposed by these stronger interactions

hold the negatively charged residues in their place. The negatively charged residues such as Asp and Glu (particularly Glu520) did show minor interactions with the positive charge of the W metals of the cage, but they were very weak and low in number (Table S1). This small interaction energy with the metals (W or Zr) was largely overshadowed by the repulsion generated as the carboxylic side chain moved closer to the oxygen cage of ZrK (Figure 2d and S4). However, an Asp/Glu residue is required in the vicinity of the Zr metal center due to its role as a Bronsted base in the acid/base chemistry utilized by POMs for peptide hydrolysis.[98] The NCI contour plots that show relative abundance and strength of the noncovalent interactions also highlighted Lys519, Arg428, Lys190, and Arg186 as the main interacting residues at this site (Figure 3a). They reveal a set of complex ZrK-HSA interactions that arise from a combination of specific atom-atom interactions including hydrogen bonding and electrostatic interactions. Furthermore, ZrK was found to form an average of 7 direct hydrogen bonds with HSA (Figure 3a). Additionally, there were multiple hydrogen bonding interactions mediated by 1-3 solvent water molecules. The key interactions promoted by one water molecule are shown in Figures 2e and 2f. In particular, the backbone of Leu115 and side chain of Arg145 associated with Zrk through one water molecule (Figure 2e). The side chains of Arg428 and Lys432 also exhibited similar interactions (Figure 2f). The catalytically important Zr-OH moiety was positioned on the interior of the protein close to this cleavage site, however, it was still exposed to water through the bottom channel opening. It was in the direct vicinity of a positively charged Lys190 residue. The binding free energy of this site was -57.5 kJ/mol (Table 1). The binding of HSA to another Kegging type POM [H2W12] was also shown to be exothermic (ΔH = -50 kJ/mol) by isothermal calorimetry (ITC) experiments.[40] The strong exothermicity of this process also suggests that these interactions are dominated by hydrogen bonding and electrostatic interactions.[40] The

binding of ZrK to HSA at site 1 was not observed to alter its secondary structure, which was dominated by α-helical conformation (67%), (Table 2). Additionally, this interaction had no effect on the overall structure of HSA and the RMSD with the ZrK free structure was only 1.16 Å (Figure S2). The binding of H2W12 POM also did not change the secondary structure of the HSA.[99] Furthermore, the overall secondary structure of HSA was found to be quite stable and did not alter upon the hydrolysis of site 1 both in the presence and absence of ZrK (Figure S3).

IIIb. ZrK-HSA interactions at site 2 (Ala257-Asp258). The second cleavage site (Ala257-Asp258, site 2) was formed by a nonpolar (Ala) and a negatively charged (Asp) residue. This site was located 34.5 Å away from site 1. It was sandwiched between two parts of a well folded section of HSA in which alpha helical secondary structure dominated (Figure 4a). Furthermore, this site was flanked by a large positively charged region that could offer stability for binding of ZrK to the HSA's surface (Figure 4b). In contrast to site 1, it was located on the surface of the protein, where large electropositive regions could accommodate binding of both small and large POMs with distinct charge, size and shape. Positive amino acid residues stabilize this site through hydrogen bonding interactions (Figure S5). Unlike site 1, the docking procedure (both rigid and flexible) around this site provided only one binding motif that was used as the starting point in the subsequent MD simulations. The most representative structure derived from MD simulations is shown in Figure 4c and d. The positively charged Arg10 associated with ZrK through two weak hydrogen bonds (Figure 4c and d). Additionally, the α-amino group of Lys262 formed two hydrogen bonds with the oxygen atoms of ZrK at distances of 2.18 and 2.71 Å. NCI contour plots also showed moderate electrostatic interactions originating from the Arg10 and Lys262 residues (Figure 3b). In comparison to site 1, at this site ZrK formed a much smaller

number of direct hydrogen bonds, on average 3, with HSA (Figure 3b). Among water mediated hydrogen bonds, the side chains of Lys240 and Lys262 interacted through one water molecule (Figure 4e). On the other hand, both side chain and backbone of Asp13 formed hydrogen bonds with the cage of Zrk (Figure 4f). Here, negatively charged Asp13 and Asp255 residues were also found to directly interact with the W atom of ZrK (Table Sx). These, rather surprising, interactions were further investigated using hybrid quantum mechanics/molecular mechanics (QM/MM) ONIOM calculation. In the starting structure of this calculation, the interactions of W with Asp13 and Asp255 were broken by flipping them out of the binding pocket (≥3.8 Å). However, during the optimization, both these residues changed their orientations and coordinated to the W metal as observed in the MD equilibrated structure. These interactions induced slight modification to the geometry of the W metal center that changed from octahedron to distorted pentagonal bipyramidal conformation.

Unlike site 1, here the Zr-OH moiety was flipped out and exposed to the solvent positioned perpendicular to the cleavage site. As a result of these weak and fewer interactions, the binding free energy (24.2 kJ/mol, Table 1) for this site was substantially higher than the one (57.5 kJ/mol) computed for site 1. The association of POM to this site slightly (1%) increased the α-helical content (69%) of HSA in comparison to site 1, but the overall secondary structure remained the same (Table 2). The binding of ZrK at this site and its hydrolysis did not modify the overall structure of HSA and RMSD remained 1.15 Å in both cases. Since binding of ZrK to sites 1 and 2 and their hydrolysis did not change the structure of HSA, those possibilities were not explored for the remaining two sites.

IIIc. ZrK-HSA interactions at site 3 (Lys313-Asp314). The third cleavage site (Lys313-Asp314, site 3) was created by a positively charged (Lys) and a negatively charged (Asp) residue. This site was located 61.4 Å apart from site 1 and positioned on the edge of HSA (Figure 5a). It contains a small positively charged patch surrounded by a predominantly negative region (Figure 5b). Since this site possesses the smallest positively charged region, the binding of larger POMs structures, except ZrK, at this location would be quite difficult. As expected, among all four cleavage sites, this site was the most challenging to obtain the ZrK-HSA complex. That was in part due to its location at the very edge of HSA with not much in the way of amino acids to stabilize this site. The lack of secondary structure within this site could also account for the loss in stabilization. Unlike for the previous two sites, for which rigid docking multiple binding motifs were observed, here mainly binding to the side of HSA near the cleavage site was detected. However, these binding sites positioned ZrK far (≥ 10 Å) from the peptide bond cleavage site and were discarded. However, flexible docking that allowed Lys313 and Lys317 to adjust their conformations provided a more stable binding site on the very edge of HSA. In this pose, ZrK was positioned much closer to the cleavage site. The MD simulations showed that at this site, ZrK was trapped between two positively charged residues Lys313 and Lys317 (Figure 5c and d). Both these residues formed multiple hydrogen bonding interactions with ZrK. In particular, the amine side chains of Lys313 and Lys317 residues associated through contacts with the oxygen cage of ZrK (Figure S6). Additionally, ZrK interacted directly with the residues forming the scissile peptide bond which was not observed for any other site. The NCI plots also showed Lys313 and Lys317 as main interacting residues and similar to site 2, ZrK formed 3 direct hydrogen bonds on average with HSA (Figure 3c). Additionally, some solvent water mediated interactions were observed for this site. For instance, side chains of Lys313 and

Asp314 associated with Zrk through one water molecule each that form a single hydrogen bond with oxygen atoms of the metal cluster (Figure 5e). On the other hand, the side chain of Lys317 formed a hydrogen bond with a water molecule that in turn interacted through two hydrogen bonds with ZrK (Figure 5f). Similar to site 2, the Zr-OH moiety in this site was oriented towards the solvent i.e. on the opposite site of the substrate. The binding free energy of -50.8 kJ/mol for this site is comparable to site 1 but much lower than the binding energy for site 2 (Table 1). The ZrK-POM association at this site is facilitated by smaller number but somewhat stronger interactions in comparison to site 1. In comparison to the previous sites, the association of ZrK to this site slightly (1%) decreased the α-helical content (66%) by 1% and 3%, respectively without affecting the overall structure of HSA (Table 2).

IIId. ZrK-HSA interactions at site 4 (Cys392-Glu393). The last site (Cys392-Glu393, site 4) was created by a nonpolar (Cys) and a negatively charged (Glu) residue. This site was positioned 33.9 Å away from site 1 on the backside of HSA. It was stabilized by alpha helical secondary structure and a cysteine bridge (Figure 6a). This binding pocket was surrounded by a very large positively charged region located next to the cleavage site (Figure 6b). Similar to site 2, this site was situated on the surface of HSA. Since it possessed the largest positive region among all four sites, it could easily accommodate different types of POMs irrespective of their charge, size, and shape. From both rigid and flexible docking, two binding motifs were observed with the first being close to the site of cleavage however was primarily stabilized by a glutamine residue. The second binding motif was located on the opposite side of the cleavage site however it was stabilized by a host of hydrogen bonds originating from positively charge residues such as Lys and Arg. Due to greater electrostatic interaction and stabilization, the second binding motif was

found to dominate and was used for the subsequent MD simulations. The binding pocket was formed primary from Arg410, Lys413, Lys414, and Lys541 all held strong hydrogen bonding interactions with the negatively charged oxygen cage of ZrK (Figure 6c and d). Interestingly, this was the largest positive patch calculated for HSA as shown be electrostatic maps. This large positively charged region could make this site more accessible to ZrK, and this was observed during the simulations. Additionally, this site has been identified as the major binding site for a variety of drug molecules such as ibuprofen[100-101] and diazepam[101-102] and has been labeled Sudlow's drug site II[103-104]. Like site 1, ZrK was held between many positive residues Arg410, Lys413, Lys414, and Lys541 of HSA at distances of 2.20, 2.26, 2.48, and 2.42 Å, respectively (Figure 6c and d). Additionally, these residues interacted through multiple hydrogen bonds with the cage of ZrK, for example, Lys414 shows hydrogen bonding interaction with three separate contacts with the oxygen cage of ZrK (Figure S7). However, the interaction distances were shorter in comparison to the other sites 2 and 3 where hydrogen bonding was weaker and less in number. This site is most comparable to site 1 where it was surrounded by positively charged residues however; site 4 is more exposed to the solvent whereas site 1 was more buried within the protein. Unlike other three sites, a water molecule was found to be very close to Zr in this site. At this location, it can directly bind to the metal ion and change its coordination number as shown by previous DFT and Car-Parrinello MD simulations.[105-106] Additionally, Glu492 formed a very weak electrostatic interaction with a W metal of ZrK at a distance of 2.92 Å (Figure 6c and Table S1). However, this weak interaction was dominated by the repulsion between the carboxylic side chain of Glu492 and the oxygen framework of ZrK (Figure S7 in supporting information). Therefore, as in all sites, there was a competition between the attractive and repulsive forces generated by positively (Lys and Arg) and negatively (Asp and Glu) charged

residues, respectively. At this site, ZrK formed the highest number of direct hydrogen bonds, 8 on average, with HSA and showed strong interactions with Lys541, Lys413, Lys414, and Arg410 (Figure 3d). Like in the first three sites, hydrogen bonding interaction involving one water molecule was observed. For instance, side chains of Gln390, Asn386, and Ser489 interact with ZrK through one water molecules (Figure 6e). Ser489 associates with this complex through unusual hydrogen bonding. The carboxyl group of this residue utilizes one water molecule to interact with ZrK (Figure 6e). Furthermore, Lys413 and Val493 interact with the oxygen framework of ZrK through one and two water molecules, respectively (Figure 6f). This site possessed the highest binding free energy (-91.2 kJ/mol, Table 1) among all four binding sites. Similar to site 1, in contrast to sites 2 and 3, the Zr-OH group here was opposite the protein's surface and was shifted towards the cleavage site. Rather surprisingly, the α-helical content (66%) of this site is exactly the same as of the site 3 (Table 2).

IV. Summary and Conclusions. In this study, we have employed molecular docking and all-atom MD simulation techniques to study interactions of 1:1 Zr-containing Keggin POM (ZrK) with four cleavage sites of HSA. These chemically diverse sites (Arg114-Leu115, Ala257-Asp258, Lys313-Asp314, and Cys392-Glu393) were located in different parts of HSA (Figure 1). They were found to bind in a rather distinct manner to form the ZrK-HSA complexes. These complexes were dominated by hydrogen bonding interactions from the oxo group containing framework of ZrK and positively charged amino acid residues of HSA. The computed binding free energies (-57.5, -24.2, -50.8, and -91.2 kJ/mol for site 1, 2 ,3 and 4, respectively) suggested that there is one major binding site (site 4), two intermediate (site 1 and site 3) and one minor binding site (site 2), Table 1. The site 4 has been known to bind several drug molecules as well.

The high exothermicity of this process was in agreement with the measured value (ΔH = -50 kJ/mol) for the POM [H2W12]-HSA interaction.[40] It is suggested to be driven mostly by electrostatic interactions.[40] At site 4, the ZrK-HSA complex formed 8 direct hydrogen bonds on average, while 2-3 direct hydrogen bonds were observed for sites 2 and 3. These hydrogen bonds were contributed by positively charged Lys and Arg residues. Additionally, there were multiple hydrogen bonding interactions mediated by 1-3 solvent water molecules. The binding of ZrK to HSA did not modify the secondary structure of HSA which was primarily dominated by α-helical conformation (67%), Table 2. Furthermore, as suggested experimentally the binding of ZrK and hydrolysis at sites 1 and 2 did not alter the overall structure of HSA.[99] POMs, in general, have been reported to interact with diverse biomolecules through hydrogen bonding albeit with varying strength, extent, and type. Our study is complementary to experimental binding studies between POMs and proteins that are typically performed with ITC or Trp fluorescence spectroscopy, however it offers an additional advantage as it allows detailed molecular and thermodynamic understanding of each binding site separately. Therefore, these results can be also applicable to understand the interaction of other POMs with a variety of different proteins.

V. Supporting Information Materials. Figures S1-S7 and Table S1. This material is available free of charge via the Internet at http://pubs.acs.org.

VI. Acknowledgements. The authors declare no competing financial interests. This material is based upon work supported by the grant from the National Science Foundation (Grant Number CHE-1664926) to R.P. Computational resources from the Center for Computational Science

(CCS) at the University of Miami to R.P. are also greatly appreciated. Additionally, T.N.P.V. thanks Research Foundation Flanders (FWO) for funding.

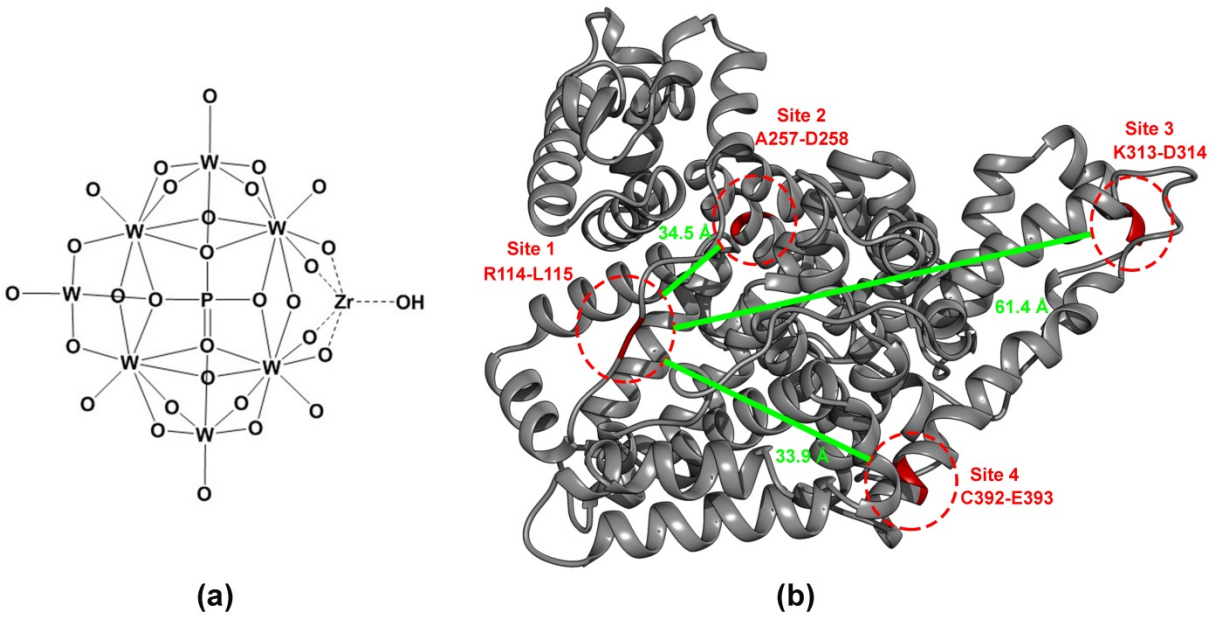

Figure 1: Structure of (a) polyoxometalate (POM) and (b) human serum albumin (HSA)

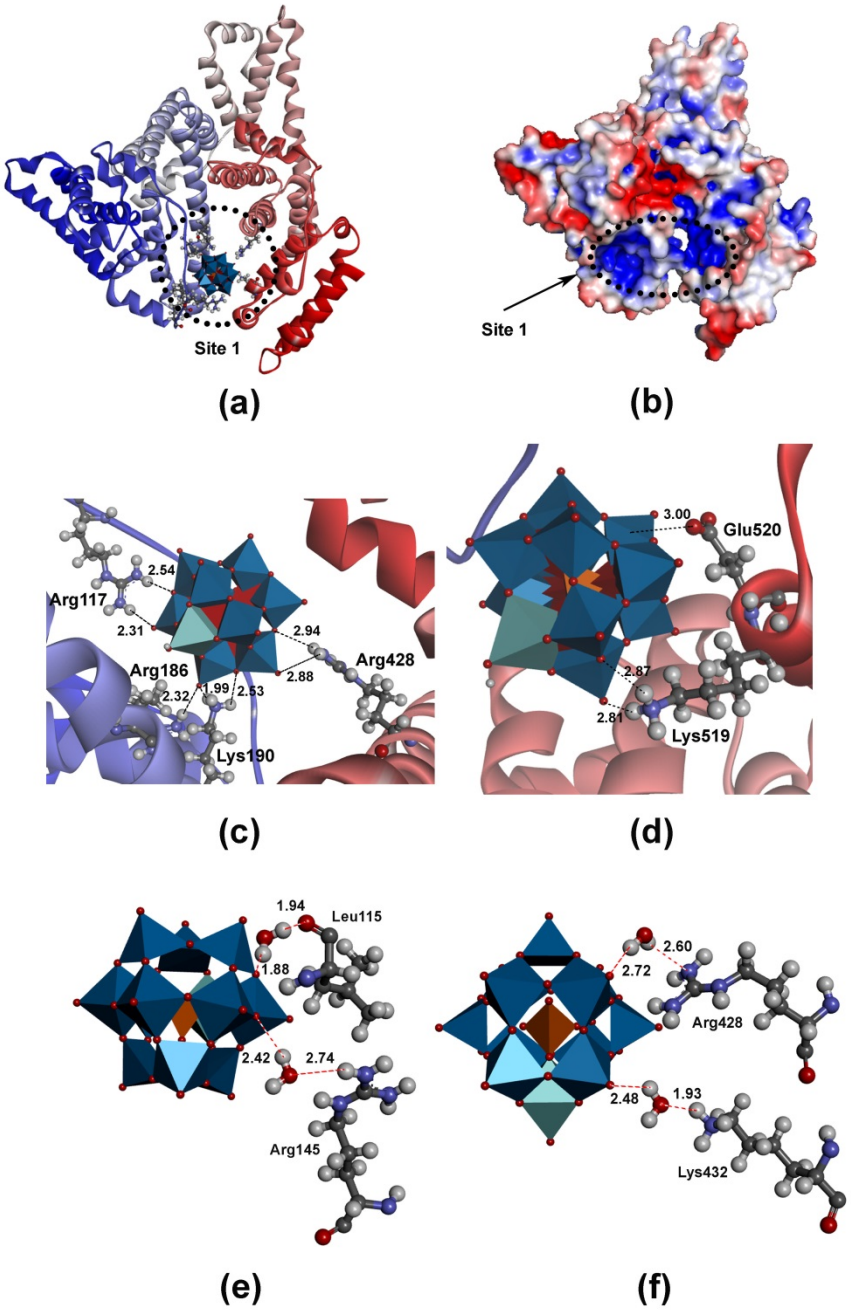

Figure 2: Most representative structure of POMs-HSA at site 1 obtained from molecular dynamics simulations: (a) the whole protein with cleavage site 1 highlighted with N and C-terminal ends colored blue and red respectively, (b) electrostatic map of HSA, (c) and (d) are zoomed in images of binding site 1 with amino acid residues and interaction distances labeled in Å, and (e) and (f) are showing water mediated interactions with the oxygen of ZrK, hydrogen bonding interacting distances labeled in Å. In the POMs structure, the orange polyhedron represents the interior phosphate group, the dark blue polyhedron represents the octahedron geometry around the tungsten, while the light blue represents the Zr(IV) species.

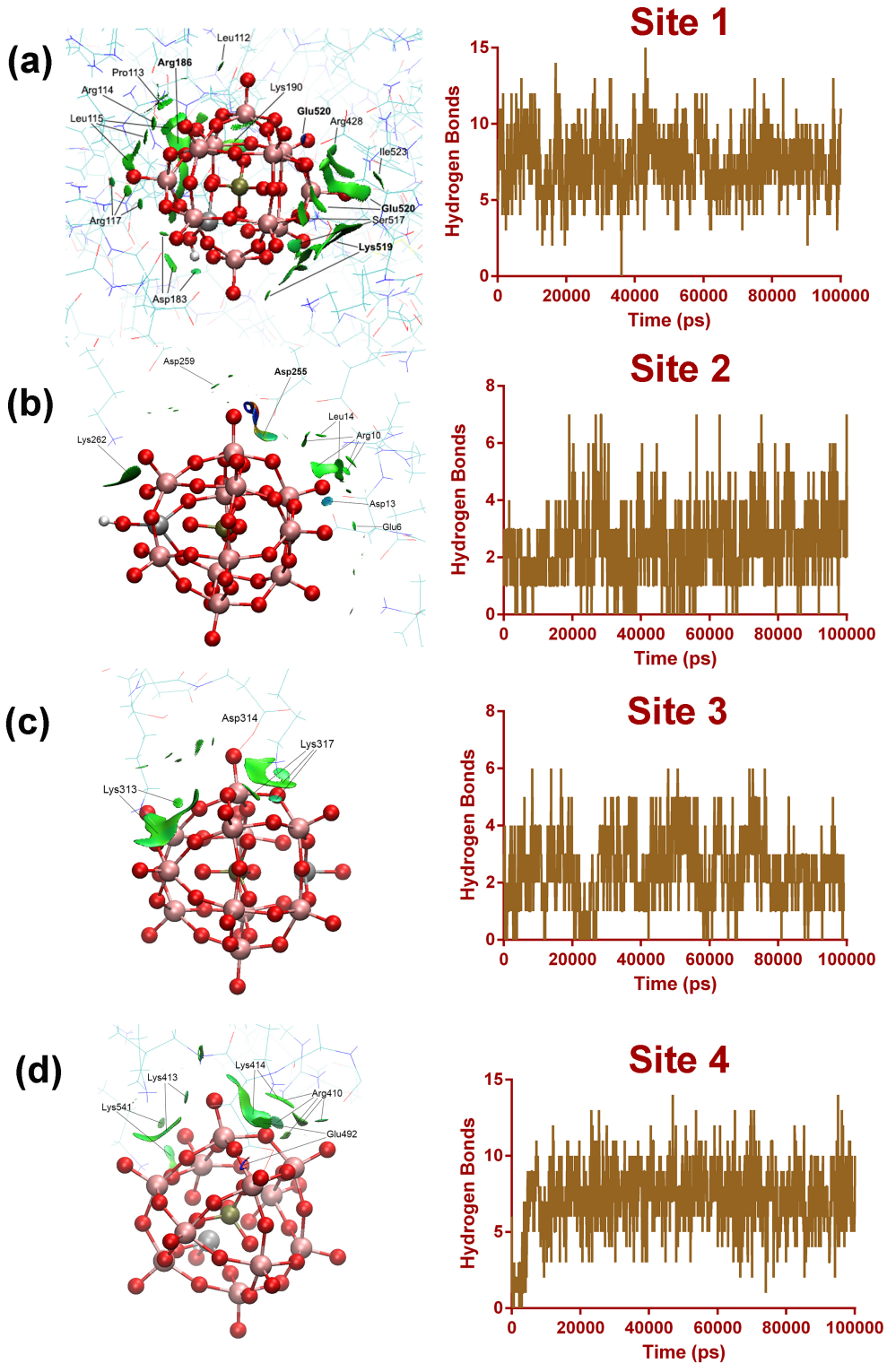

Figure 3: Noncovalent interaction (NCI) plots and hydrogen bonding interactions at all four sites.

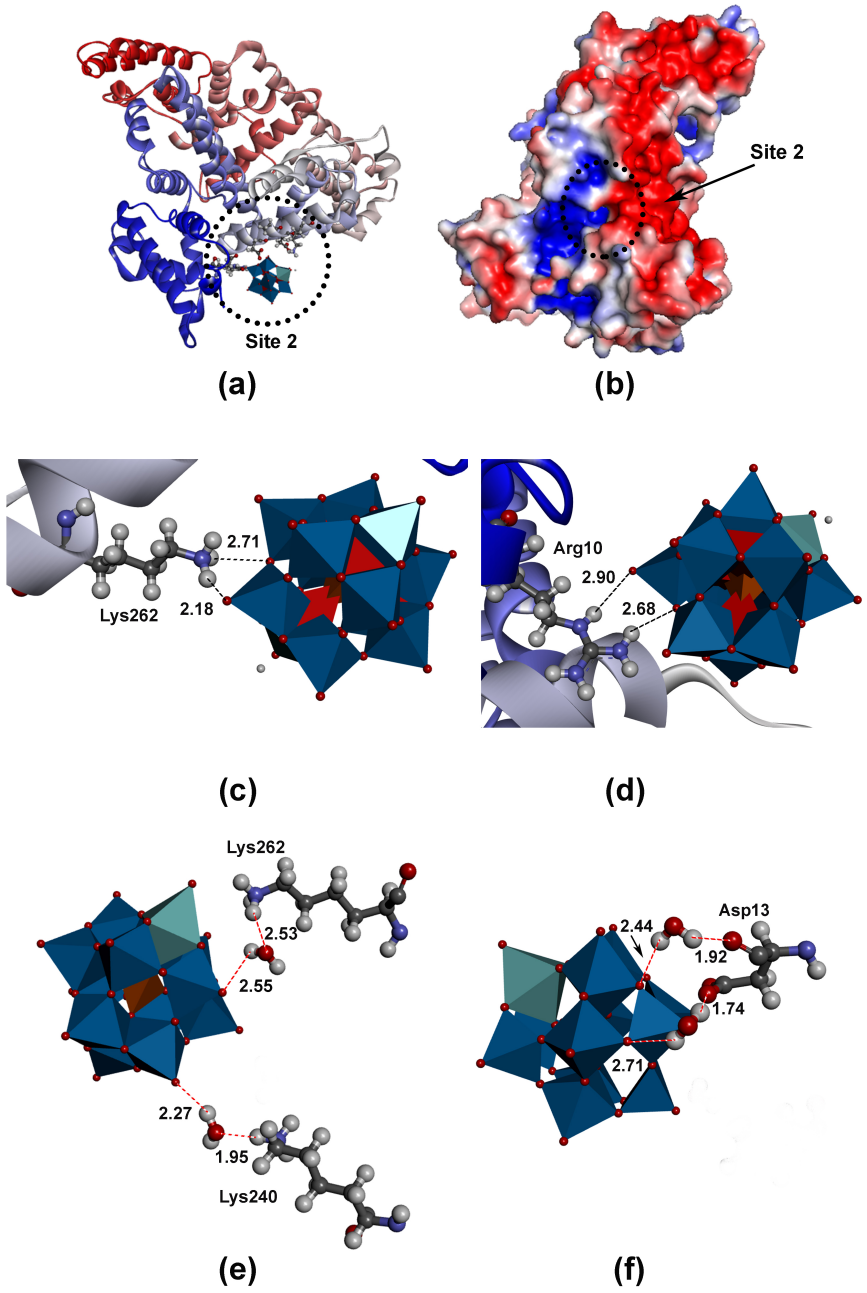

Figure 4: Most representative structure of POMs-HSA at site 2 obtained from molecular dynamics simulations: (a) the whole protein with cleavage site 2 highlighted with N and C-terminal ends colored blue and red respectively, (b) electrostatic map of HSA, (c) and (d) are zoomed in images of binding site 2 with amino acid residues and interaction distances labeled in Å, and (e) and (f) are showing water mediated interactions with the oxygen of ZrK, hydrogen bonding interacting distances labeled in Å. In the POMs structure, the orange polyhedron represents the interior phosphate group, the dark blue polyhedron represents the octahedron geometry around the tungsten, while the light blue represents the Zr(IV) species.

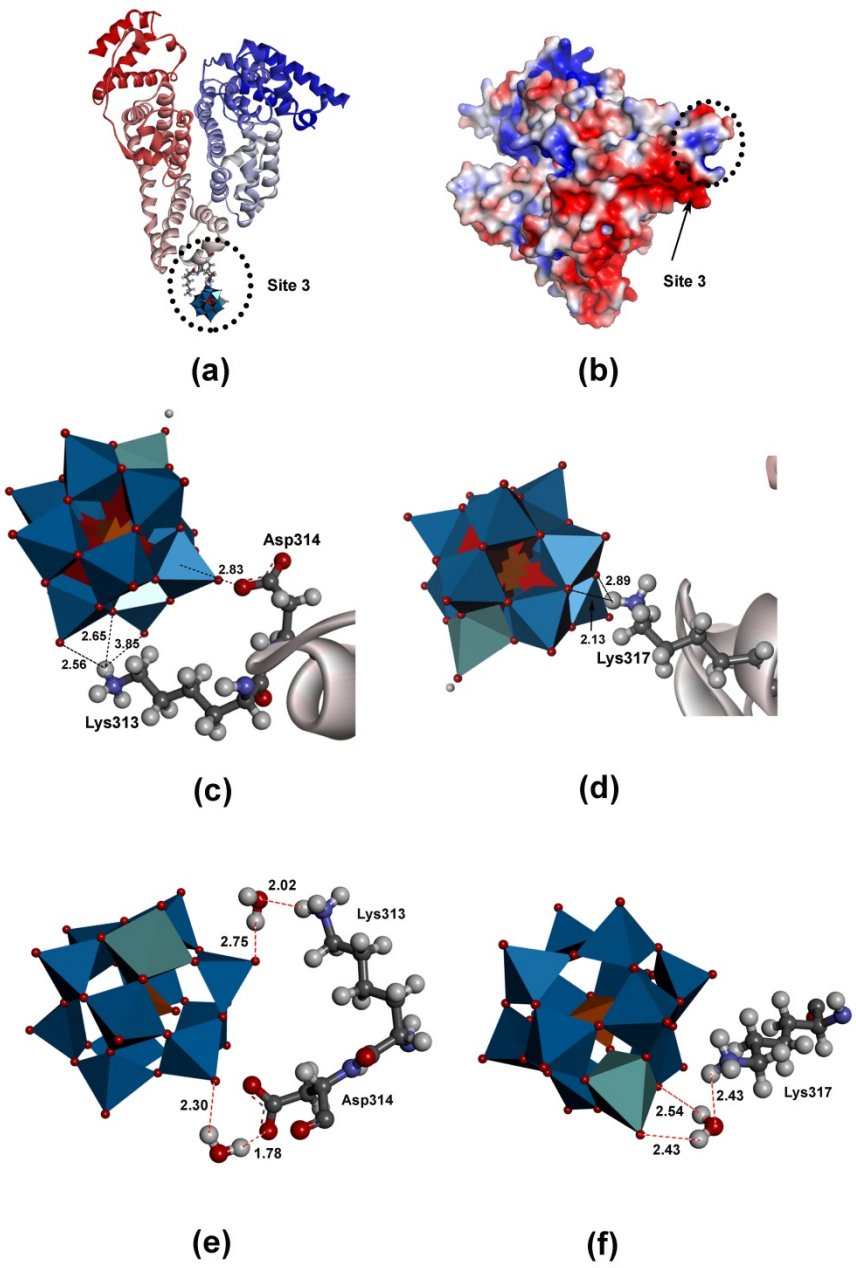

Figure 5: Most representative structure of POMs-HSA at site 3 obtained from molecular dynamics simulations: (a) the whole protein with cleavage site 3 highlighted with N and C-terminal ends colored blue and red respectively, (b) electrostatic map of HSA, (c) and (d) are zoomed in images of binding site 3 with amino acid residues and interaction distances labeled in Å, and (e) and (f) are showing water mediated interactions with the oxygen of ZrK, hydrogen bonding interacting distances labeled in Å. In the POMs structure, the orange polyhedron represents the interior phosphate group, the dark blue polyhedron represents the octahedron geometry around the tungsten, while the light blue represents the Zr(IV) species.

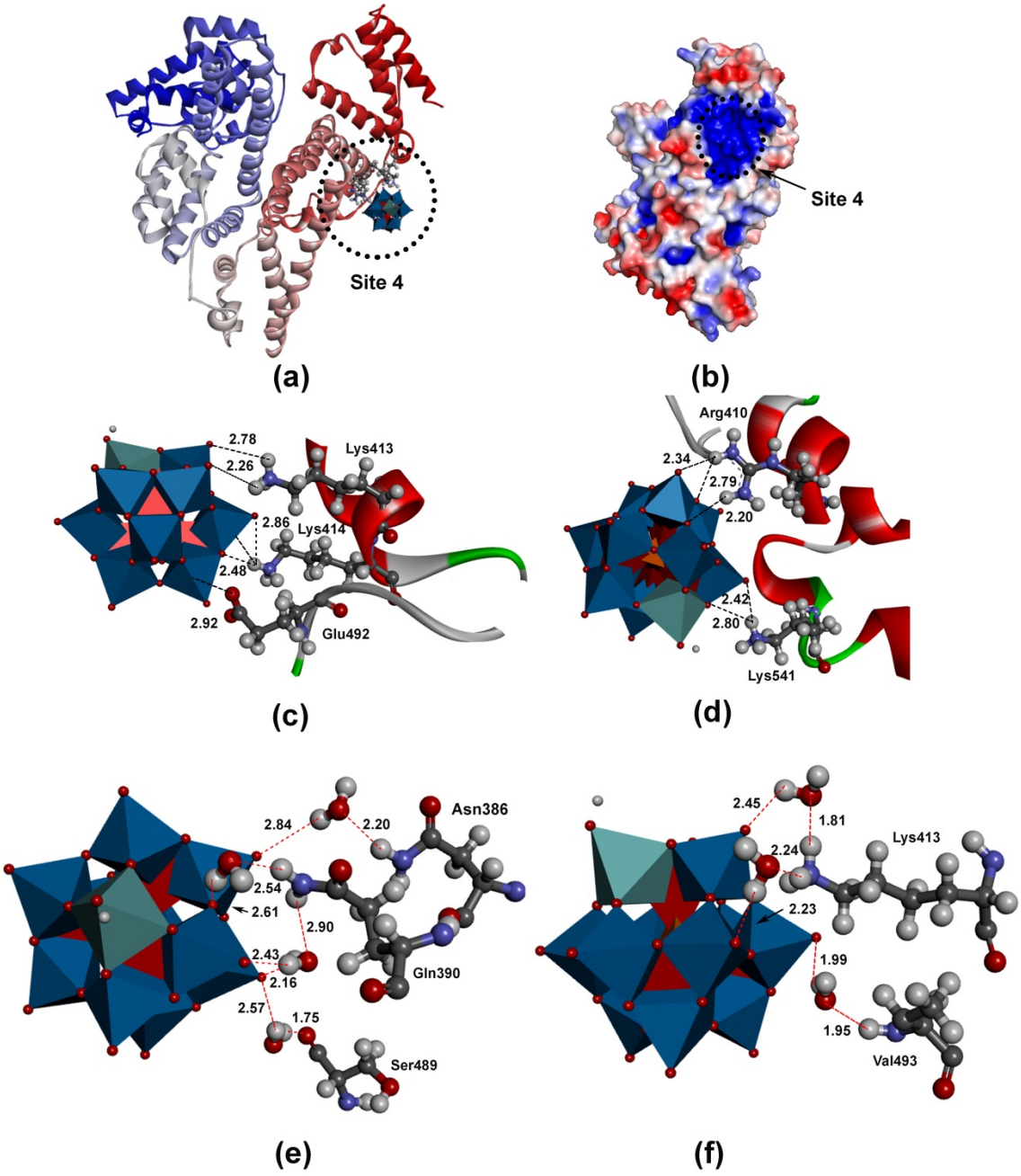

Figure 6: Most representative structure of POMs-HSA at site 4 obtained from molecular dynamics simulations: (a) the whole protein with cleavage site 4 highlighted with N and C-terminal ends colored blue and red respectively, (b) electrostatic map of HSA, (c) and (d) are zoomed in images of binding site 4 with amino acid residues and interaction distances labeled in Å, and (e) and (f) are showing water mediated interactions with the oxygen of ZrK, hydrogen bonding interacting distances labeled in Å. In the POMs structure, the orange polyhedron represents the interior phosphate group, the dark blue polyhedron represents the octahedron geometry around the tungsten, while the light blue represents the Zr(IV) species.

Position	Hydrogen Bonds	$\Delta G_{Binding}$
Site 1	7	-57.5 ± 11.7
Site 2	3	-24.2 ± 11.9
Site 3	3	-50.8 ± 11.3
Site 4	8	-91.2 ± 10.8

Table 1: Free energy change of the complexation of the ligand and receptor (kJ/mol).

Position	Coil	Bend	Turn	A-Helix	3-Helix
HSA	13	8	9	68	2
Site 1	13	6	9	67	5
Site 2	13	6	9	69	3
Site 3	13	7	10	66	4
Site 4	13	6	10	66	5

Table 2: Secondary structure (%) of Human Serum Albumin (HSA) and POMs bound to HSA at sites 1-4.

References:

(1) Stroobants, K.; Absillis, G.; Moelants, E.; Proost, P.; Parac-Vogt, T. N., Regioselective Hydrolysis of Human Serum Albumin by Zr(IV)-Substituted Polyoxotungstates at the Interface of Positively Charged Protein Surface Patches and Negatively Charged Amino Acid Residues. *Chem. - Eur. J.* **2014,** *20*, 3894-3897.

(2) Proust, A.; Thouvenot, R.; Gouzerh, P., Functionalization of Polyoxometalates: Towards Advanced Applications in Catalysis and Materials Science. *Chem. Commun.* **2008**, 1837-1852.

(3) Long, D.-L.; Tsunashima, R.; Cronin, L., Polyoxometalates: Building Blocks for Functional Nanoscale Systems. *Angew. Chem., Int. Ed.* **2010,** *49*, 1736-1758.

(4) Bard, A.; Stratmann, M.; Scholz, F.; Pickett, C., *Electrochemistry of Isopoly and Heteropoly Oxometalates*. Wiley-VCH Verlag GmbH & Co.: In Encyclopedia of Electrochemistry, A. J. Bard (Ed.). Weinheim, Germany. 2007; Vol. 7.

(5) Zhang, G.; Yang, W.; Yao, J., Thermally Enhanced Visible-Light Photochromism of Phosphomolybdic Acid–Polyvinylpyrrolidone Hybrid Films. *Adv. Funct. Mater.* **2005,** *15*, 1255-1259.

(6) Zhang, G.; Chen, Z.; He, T.; Ke, H.; Ma, Y.; Shao, K.; Yang, W.; Yao, J., Construction of Self-Assembled Ultrathin Polyoxometalate/1,10-Decanediamine Photochromic Films. *J. Phys. Chem. B* **2004,** *108*, 6944-6948.

(7) Glass, E. N.; Fielden, J.; Huang, Z.; Xiang, X.; Musaev, D. G.; Lian, T.; Hill, C. L., Transition Metal Substitution Effects on Metal-to-Polyoxometalate Charge Transfer. *Inorg. Chem.* **2016,** *55*, 4308-4319.

(8) Piot, M.; Hupin, S.; Lavanant, H.; Afonso, C.; Bouteiller, L.; Proust, A.; Izzet, G., Charge Effect on the Formation of Polyoxometalate-Based Supramolecular Polygons Driven by Metal Coordination. *Inorg. Chem.* **2017,** *56*, 8490-8496.

(9) McGregor, D.; Burton-Pye, B. P.; Mbomekalle, I. M.; Aparicio, P. A.; Romo, S.; López, X.; Poblet, J. M.; Francesconi, L. C., 99tc and Re Incorporated into Metal Oxide Polyoxometalates: Oxidation State Stability Elucidated by Electrochemistry and Theory. *Inorg. Chem.* **2012,** *51*, 9017-9028.

(10) Sarma, B. B.; Neumann, R., Polyoxometalate-Mediated Electron Transfer–Oxygen Transfer Oxidation of Cellulose and Hemicellulose to Synthesis Gas. *Nat. Comm.* **2014,** *5*, 4621.

(11) Eynat, H.; W., S. L. J.; Ronny, N., Photochemical Reduction of CO_2 with Visible Light Using a Polyoxometalate as Photoreductant. *Chem. Eur. J.* **2017,** *23*, 92-95.

(12) Bernardini, G.; Wedd, A. G.; Zhao, C.; Bond, A. M., Photochemical Oxidation of Water and Reduction of Polyoxometalate Anions at Interfaces of Water with Ionic Liquids or Diethylether. *Proc. Natl. Acad. Sci. U. S. A.* **2012,** *109*, 11552-11557.

(13) Wang, J.; Liu, Y.; Xu, K.; Qi, Y.; Zhong, J.; Zhang, K.; Li, J.; Wang, E.; Wu, Z.; Kang, Z., Broad-Spectrum Antiviral Property of Polyoxometalate Localized on a Cell Surface. *ACS Appl Mater Interfaces* **2014,** *6*, 9785-9789.

(14) Lei, F.; Hanqin, G.; Mei, Y.; Shouzhu, L.; Xinyu, L.; Zhifei, D.; Shaoqin, L., Polyoxometalate-Based Organic–Inorganic Hybrids as Antitumor Drugs. *Small* **2015,** *11*, 2938-2945.

(15) Sansom, F. M.; Riedmaier, P.; Newton, H. J.; Dunstone, M. A.; Müller, C. E.; Stephan, H.; Byres, E.; Beddoe, T.; Rossjohn, J.; Cowan, P. J., et al., Enzymatic Properties of an Ecto-

Nucleoside Triphosphate Diphosphohydrolase from Legionella Pneumophila: Substrate Specificity and Requirement for Virulence. *J. Biol. Chem.* **2008,** *283*, 12909-12918.

(16) Zhang, Z.-M.; Duan, X.; Yao, S.; Wang, Z.; Lin, Z.; Li, Y.-G.; Long, L.-S.; Wang, E.-B.; Lin, W., Cation-Mediated Optical Resolution and Anticancer Activity of Chiral Polyoxometalates Built from Entirely Achiral Building Blocks. *Chem. Sci.* **2016,** *7*, 4220-4229.

(17) Bijelic, A.; Rompel, A., The Use of Polyoxometalates in Protein Crystallography – an Attempt to Widen a Well-Known Bottleneck. *Coord. Chem. Rev.* **2015,** *299*, 22-38.

(18) Wang, X.; Wang, J.; Zhang, W.; Li, B.; Zhu, Y.; Hu, Q.; Yang, Y.; Zhang, X.; Yan, H.; Zeng, Y., Inhibition of Human Immunodeficiency Virus Type 1 Entry by a Keggin Polyoxometalate. *Viruses* **2018,** *10*, 265.

(19) Flütsch, A.; Schroeder, T.; Grütter, M. G.; Patzke, G. R., HIV-1 Protease Inhibition Potential of Functionalized Polyoxometalates. *Bioorg Med Chem Lett* **2011,** *21*, 1162-1166.

(20) Geng, J.; Li, M.; Ren, J.; Wang, E.; Qu, X., Polyoxometalates as Inhibitors of the Aggregation of Amyloid β Peptides Associated with Alzheimer's Disease. *Angew. Chem., Int. Ed.* **2011,** *50*, 4184-4188.

(21) Pu, F.; Wang, E.; Jiang, H.; Ren, J., Identification of Polyoxometalates as Inhibitors of Basic Fibroblast Growth Factor. *Mol. BioSyst.* **2013,** *9*, 113-120.

(22) Stroobants, K.; Goovaerts, V.; Absillis, G.; Bruylants, G.; Moelants, E.; Proost, P.; Parac-Vogt, T. N., Molecular Origin of the Hydrolytic Activity and Fixed Regioselectivity of a Zr(IV)-Substituted Polyoxotungstate as Artificial Protease. *Chem. - Eur. J.* **2014,** *20*, 9567-9577.

(23) Stroobants, K.; Moelants, E.; Ly, H. G. T.; Proost, P.; Bartik, K.; Parac-Vogt, T. N., Polyoxometalates as a Novel Class of Artificial Proteases: Selective Hydrolysis of Lysozyme

under Physiological PH and Temperature Promoted by a Cerium(IV) Keggin-Type Polyoxometalate. *Chem. - Eur. J.* **2013,** *19*, 2848-2858.

(24) Ly, H. G. T.; Parac-Vogt, T. N., Spectroscopic Study of the Interaction between Horse Heart Myoglobin and Zirconium(IV)-Substituted Polyoxometalates as Artificial Proteases. *ChemPhysChem* **2017,** *18*, 2451-2458.

(25) Sap, A.; Van Tichelen, L.; Mortier, A.; Proost, P.; Parac-Vogt, T. N., Tuning the Selectivity and Reactivity of Metal-Substituted Polyoxometalates as Artificial Proteases by Varying the Nature of the Embedded Lewis Acid Metal Ion. *Eur. J. Inorg. Chem.* **2016,** *2016*, 5098-5105.

(26) Radzicka, A.; Wolfenden, R., Rates of Uncatalyzed Peptide Bond Hydrolysis in Neutral Solution and the Transition State Affinities of Proteases. *J. Am. Chem. Soc.* **1996,** *118*, 6105-6109.

(27) Song, W.; Han, X.; Qian, Y.; Liu, G.; Yao, G.; Zhong, Y.; Qu, Y., Proteomic Analysis of the Biomass Hydrolytic Potentials of Penicillium Oxalicum Lignocellulolytic Enzyme System. *Biotechnol Biofuels* **2016,** *9*, 68.

(28) Kopera, E.; Krężel, A.; Protas, A. M.; Belczyk, A.; Bonna, A.; Wysłouch-Cieszyńska, A.; Poznański, J.; Bal, W., Sequence-Specific Ni(II)-Dependent Peptide Bond Hydrolysis for Protein Engineering: Reaction Conditions and Molecular Mechanism. *Inorg. Chem.* **2010,** *49*, 6636-6645.

(29) Wang, L.; Chance, M. R., Protein Footprinting Comes of Age: Mass Spectrometry for Biophysical Structure Assessment. *Mol. Cell. Proteomics* **2017,** *16*, 706-716.

(30) Zhang, H.; Wen, J.; Huang, R. Y. C.; Blankenship, R. E.; Gross, M. L., Mass Spectrometry-Based Carboxyl Footprinting of Proteins: Method Evaluation. *Int. J. Mass Spectrom* **2012,** *312*, 78-86.

(31) Xu, H.; Yang, X.; Xie, L.; Hakkarainen, M., Conformational Footprint in Hydrolysis-Induced Nanofibrillation and Crystallization of Poly(Lactic Acid). *Biomacromolecules* **2016,** *17*, 985-995.

(32) Sakakura, M.; Takayama, M., Sonolytic Hydrolysis of Peptides in Aqueous Solution Upon Addition of Catechol. *Ultrason. Sonochem.* **2009,** *16*, 367-371.

(33) O'Keeffe, M. B.; FitzGerald, R. J., Identification of Short Peptide Sequences in Complex Milk Protein Hydrolysates. *Food Chem.* **2015,** *184*, 140-146.

(34) López, C. M.; Bru, E.; Vignolo, G. M.; Fadda, S. G., Identification of Small Peptides Arising from Hydrolysis of Meat Proteins in Dry Fermented Sausages. *Meat Science* **2015,** *104*, 20-29.

(35) Burton, A. J.; Thomson, A. R.; Dawson, W. M.; Brady, R. L.; Woolfson, D. N., Installing Hydrolytic Activity into a Completely *De Novo* Protein Framework. *Nat. Chem.* **2016,** *8*, 837.

(36) Galante, Y. M.; Formantici, C., Enzyme Applications in Detergency and Manufacturing Industries. *Curr. Org. Chem.* **2003,** *7*, 1399-1422.

(37) Lee, T. Y.; Suh, J., Target-Selective Peptide-Cleaving Catalysts as a New Paradigm in Drug Design. *Chem. Soc. Rev.* **2009,** *38*, 1949-1957.

(38) Priyanka, B.; Gopeekrishnan, S.; Vikas, T.; Rudi, F., Gram-Scale Synthesis of Chiral Cyclopropane-Containing Drugs and Drug Precursors with Engineered Myoglobin Catalysts Featuring Complementary Stereoselectivity. *Angew. Chem., Int. Ed.* **2016,** *55*, 16110-16114.

(39) Zheng, L.; Ma, Y.; Zhang, G.; Yao, J.; Keita, B.; Nadjo, L., A Multitechnique Study of Europium Decatungstate and Human Serum Albumin Molecular Interaction. *Phys. Chem. Chem. Phys.* **2010,** *12*, 1299-1304.

(40) Zhang, G.; Keita, B.; Craescu, C. T.; Miron, S.; de Oliveira, P.; Nadjo, L., Polyoxometalate Binding to Human Serum Albumin: A Thermodynamic and Spectroscopic Approach. *J. Phys. Chem. B* **2007,** *111*, 11253-11259.

(41) Zhang, G.; Keita, B.; Craescu, C. T.; Miron, S.; de Oliveira, P.; Nadjo, L., Molecular Interactions between Wells−Dawson Type Polyoxometalates and Human Serum Albumin. *Biomacromolecules* **2008,** *9*, 812-817.

(42) Lopez, X.; Carbo, J. J.; Bo, C.; Poblet, J. M., Structure, Properties and Reactivity of Polyoxometalates: A Theoretical Perspective. *Chem. Soc. Rev.* **2012,** *41*, 7537-7571.

(43) López, X.; Miró, P.; Carbó, J. J.; Rodríguez-Fortea, A.; Bo, C.; Poblet, J. M., Current Trends in the Computational Modelling of Polyoxometalates. *Theor. Chem. Acc.* **2011,** *128*, 393-404.

(44) Solé-Daura, A.; Goovaerts, V.; Stroobants, K.; Absillis, G.; Jiménez-Lozano, P.; Poblet, J. M.; Hirst, J. D.; Parac-Vogt, T. N.; Carbó, J. J., Probing Polyoxometalate–Protein Interactions Using Molecular Dynamics Simulations. *Chem. - Eur. J.* **2016,** *22*, 15280-15289.

(45) Ferraro, G.; Massai, L.; Messori, L.; Merlino, A., Cisplatin Binding to Human Serum Albumin: A Structural Study. *Chem. Commun.* **2015,** *51*, 9436-9439.

(46) He, X. M.; Carter, D. C., Atomic Structure and Chemistry of Human Serum Albumin. *Nature* **1992,** *358*, 209-215.

(47) Carter, D. C.; Ho, J. X., Structure of Serum Albumin. *Adv. Protein Chem.* **1994,** *45*, 153-203.

(48) Peters, T., *All About Albumin*. Academic Press: New York, 1996.

(49) Olson, R. E.; Christ, D. D., Chapter 33. Plasma Protein Binding of Drugs. *Annu. Rep. Med. Chem.* **1996,** *31*, 327-336.

(50) Boglio, C.; Hasenknopf, B.; Lenoble, G.; Rémy, P.; Gouzerh, P.; Thorimbert, S.; Lacôte, E.; Malacria, M.; Thouvenot, R., Sensing the Chirality of Dawson Lanthanide Polyoxometalates $[\alpha 1\text{-}LnP_2W_{17}O_{61}]^{7-}$ by Multinuclear Nmr Spectroscopy. *Chem. - Eur. J.* **2008,** *14*, 1532-1540.

(51) Dupré, N.; Rémy, P.; Micoine, K.; Boglio, C.; Thorimbert, S.; Lacôte, E.; Hasenknopf, B.; Malacria, M., Chemoselective Catalysis with Organosoluble Lewis Acidic Polyoxotungstates. *Chem. - Eur. J.* **2010,** *16*, 7256-7264.

(52) Goovaerts, V.; Stroobants, K.; Absillis, G.; Parac-Vogt, T. N., Molecular Interactions between Serum Albumin Proteins and Keggin Type Polyoxometalates Studied Using Luminescence Spectroscopy. *Phys. Chem. Chem. Phys.* **2013,** *15*, 18378-18387.

(53) Sap, A.; De Zitter, E.; Van Meervelt, L.; Parac-Vogt, T. N., Structural Characterization of the Complex between Hen Egg-White Lysozyme and Zr(IV)-Substituted Keggin Polyoxometalate as Artificial Protease. *Chem. - Eur. J.* **2015,** *21*, 11692-11695.

(54) Wang, Y.; Yu, H.; Shi, X.; Luo, Z.; Lin, D.; Huang, M., Structural Mechanism of Ring-Opening Reaction of Glucose by Human Serum Albumin. *J. Biol. Chem.* **2013,** *288*, 15980-15987.

(55) Becke, A. D., Density-Functional Thermochemistry. III. The Role of Exact Exchange. *J. Chem. Phys.* **1993,** *98*, 5648-5652.

(56) Hay, P. J.; Wadt, W. R., Ab Initio Effective Core Potentials for Molecular Calculations. Potentials for the Transition Metal Atoms Sc to Hg. *J. Chem. Phys.* **1985,** *82*, 270-283.

(57) Rassolov, V. A.; Ratner, M. A.; Pople, J. A.; Redfern, P. C.; Curtiss, L. A., 6-31g* Basis Set for Third-Row Atoms. *J. Comput. Chem.* **2001,** *22*, 976-984.

(58) Frisch, M. J.; Trucks, G. W.; Schlegel, H. B.; Scuseria, G. E.; Robb, M. A.; Cheeseman, J. R.; Scalmani, G.; Barone, V.; Mennucci, B.; Petersson, G. A., et al. *Gaussian 09*, Gaussian, Inc.: Wallingford, CT, USA, 2009.

(59) Trott, O.; Olson, A. J., Autodock Vina: Improving the Speed and Accuracy of Docking with a New Scoring Function, Efficient Optimization and Multithreading. *J. Comput. Chem.* **2010,** *31* 455-461.

(60) Oostenbrink, C.; Villa, A.; Mark, A. E.; Van Gunsteren, W. F., A Biomolecular Force Field Based on the Free Enthalpy of Hydration and Solvation: The Gromos Force-Field Parameter Sets 53a5 and 53a6. *J. Comput. Chem.* **2004,** *25*, 1656-1676.

(61) Lindahl, E.; Hess, B.; van der Spoel, D., Gromacs 3.0: A Package for Molecular Simulation and Trajectory Analysis. *J. Mol. Model.* **2001,** *7*, 306-317.

(62) Case, D. A.; Cheatham, T. E.; Darden, T.; Gohlke, H.; Luo, R.; Merz, K. M.; Onufriev, A.; Simmerling, C.; Wang, B.; Woods, R., The AMBER Biomolecular Simulation Programs. *J. Computat. Chem.* **2005,** *26*, 1668-1688.

(63) Wang, J.; Wang, W.; Kollman, P. A.; Case, D. A., Automatic Atom Type and Bond Type Perception in Molecular Mechanical Calculations. *J. Mol. Graphics Modell.* **2006,** *25*, 247-260.

(64) Wang, J.; Wolf, R. M.; Caldwell, J. W.; Kollman, P. A.; Case, D. A., Development and Testing of a General AMBER Force Field. *J. Comput. Chem.* **2004,** *25*, 1157-1174.

(65) Case, D. A.; Betz, R. M.; Botello-Smith, W.; Cerutti, D. S.; Cheatham, T. E.; Darden, T. A.; Duke, R. E.; Giese, T. J.; Gohlke, H.; Goetz, A. W., et al. *AMBER*, University of California, San Francisco: 2016.

(66) Leroy, F.; Miró, P.; Poblet, J. M.; Bo, C.; Bonet Ávalos, J., Keggin Polyoxoanions in Aqueous Solution: Ion Pairing and Its Effect on Dynamic Properties by Molecular Dynamics Simulations. *J. Phys. Chem. B* **2008,** *112*, 8591-8599.

(67) López, X.; Nieto-Draghi, C.; Bo, C.; Avalos, J. B.; Poblet, J. M., Polyoxometalates in Solution: Molecular Dynamics Simulations on the α-$PW_{12}O_{40}^{3-}$ Keggin Anion in Aqueous Media. *J. Phys. Chem. A* **2005,** *109*, 1216-1222.

(68) Rappe, A. K.; Casewit, C. J.; Colwell, K. S.; Goddard, W. A.; Skiff, W. M., Uff, a Full Periodic Table Force Field for Molecular Mechanics and Molecular Dynamics Simulations. *J. Am. Chem. Soc.* **1992,** *114*, 10024-10035.

(69) Jorgensen, W. L.; Chandrasekhar, J.; Madura, J. D.; Impey, R. W.; Klein, M. L., Comparison of Simple Potential Functions for Simulating Liquid Water. *J. Chem. Phys.* **1983,** *79*, 926-935.

(70) Miyamoto, S.; Kollman, P. A., Settle - an Analytical Version of the Shake and Rattle Algorithm for Rigid Water Models. *J. Comput. Chem.* **1992,** *13*, 952-962.

(71) Hess, B.; Bekker, H.; Berendsen, H. J. C.; Fraaije, J. G. E. M., Lincs: A Linear Constraint Solver for Molecular Simulations. *J. Comput. Chem.* **1997,** *18*, 1463-1472.

(72) Darden, T.; York, D.; Pedersen, L., Particle Mesh Ewald: An N·Log(N) Method for Ewald Sums in Large Systems. *J. Chem. Phys.* **1993,** *98*, 10089-10092.

(73) Contreras-García, J.; Johnson, E. R.; Keinan, S.; Chaudret, R.; Piquemal, J.-P.; Beratan, D. N.; Yang, W., Nciplot: A Program for Plotting Noncovalent Interaction Regions. *J. Chem. Theory Comput.* **2011,** *7*, 625-632.

(74) Johnson, E. R.; Keinan, S.; Mori-Sánchez, P.; Contreras-García, J.; Cohen, A. J.; Yang, W., Revealing Noncovalent Interactions. *J. Am. Chem. Soc.* **2010,** *132*, 6498-6506.

(75) Knight, J. L.; Brooks, C. L., λ-Dynamics Free Energy Simulation Methods. *J. Comput. Chem.* **2009,** *30*, 1692-1700.

(76) Kong, X.; III, C. L. B., λ-Dynamics: A New Approach to Free Energy Calculations. *J. Chem. Phys.* **1996,** *105*, 2414-2423.

(77) Guo, Z.; Brooks, C. L.; Kong, X., Efficient and Flexible Algorithm for Free Energy Calculations Using the λ-Dynamics Approach. *J. Phys. Chem. B* **1998,** *102*, 2032-2036.

(78) van Gunsteren, W. F.; Berendsen, H. J. C., Algorithms for Macromolecular Dynamics and Constraint Dynamics. *Mol. Phys.* **1977,** *34*, 1311-1327.

(79) van Gunsteren, W. F.; Berendsen, H. J. C., Algorithms for Brownian Dynamics. *Mol. Phys.* **1982,** *45*, 637-647.

(80) Van Gunsteren, W. F.; Berendsen, H. J. C., A Leap-Frog Algorithm for Stochastic Dynamics. *Mol. Simul.* **1988,** *1*, 173-185.

(81) Parrinello, M.; Rahman, A., Polymorphic Transitions in Single Crystals: A New Molecular Dynamics Method. *J. Appl. Phys.* **1981,** *52*, 7182-7190.

(82) Joosten, R. P.; te Beek, T. A. H.; Krieger, E.; Hekkelman, M. L.; Hooft, R. W. W.; Schneider, R.; Sander, C.; Vriend, G., A Series of PDB Related Databases for Everyday Needs. *Nucleic Acids Res.* **2011,** *39*, D411-D419.

(83) Kabsch, W.; Sander, C., Dictionary of Protein Secondary Structure: Pattern Recognition of Hydrogen-Bonded and Geometrical Features. *Biopolymers* **1983,** *22*, 2577-2637.

(84) Baker, N. A.; Sept, D.; Joseph, S.; Holst, M. J.; McCammon, J. A., Electrostatics of Nanosystems: Application to Microtubules and the Ribosome. *Proc. Natl. Acad. Sci. U. S. A.* **2001,** *98*, 10037-10041.

(85) PyMOL *The Pymol Molecular Graphics System* 1.8; Schrodinger LLC: 2015.

(86) Krieger, E.; Vriend, G., Models@Home: Distributed Computing in Bioinformatics Using a Screensaver Based Approach. *Bioinformatics* **2002,** *18*, 315-318.

(87) Monsonego, A.; Zota, V.; Karni, A.; Krieger, J. I.; Bar-Or, A.; Bitan, G.; Budson, A. E.; Sperling, R.; Selkoe, D. J.; Weiner, H. L., Increased T Cell Reactivity to Amyloid Beta Protein in Older Humans and Patients with Alzheimer Disease. *J. Clin. Invest.* **2003,** *112*, 415-422.

(88) Pettersen, E. F.; Goddard, T. D.; Huang, C. C.; Couch, G. S.; Greenblatt, D. M.; Meng, E. C.; Ferrin, T. E., Ucsf Chimera—a Visualization System for Exploratory Research and Analysis. *J. Comput. Chem.* **2004,** *25*, 1605-1612.

(89) Vreven, T.; Morokuma, K.; Farkas, Ö.; Schlegel, H. B.; Frisch, M. J., Geometry Optimization with QM/MM, ONIOM, and Other Combined Methods. I. Microiterations and Constraints. *J. Comp. Chem.* **2003,** *24*, 760-769.

(90) Becke, A. D., Density-Functional Exchange-Energy Approximation with Correct Asymptotic Behavior. *Phys. Rev. A* **1988,** *38*, 3098-3100.

(91) Hay, P. J.; Wadt, W. R., *Ab Initio* Effective Core Potentials for Molecular Calculations. Potentials for the Transition Metal Atoms Sc to Hg. *J. Chem. Phys.* **1985,** *82*, 270-283.

(92) Ponder, J. W.; Case, D. A., Force Fields for Protein Simulations. *Adv Protein Chem.* **2003,** *66*, 27-85.

(93) Yong, D.; Chun, W.; Shibasish, C.; C., L. M.; Guoming, X.; Wei, Z.; Rong, Y.; Piotr, C.; Ray, L.; Taisung, L., et al., A Point-Charge Force Field for Molecular Mechanics Simulations of Proteins Based on Condensed-Phase Quantum Mechanical Calculations. *J. Comput. Chem.* **2003,** *24*, 1999-2012.

(94) Spector, A. A., Fatty Acid Binding to Plasma Albumin. *J. Lipid Res.* **1975,** *16*, 165-179.

(95) Zhang, T.; Li, H.-W.; Wu, Y.; Wang, Y.; Wu, L., The Two-Step Assemblies of Basic-Amino-Acid-Rich Peptide with a Highly Charged Polyoxometalate. *Chem. - Eur. J.* **2015,** *21*, 9028-9033.

(96) Li, H.-W.; Wang, Y.; Zhang, T.; Wu, Y.; Wu, L., Selective Binding of Amino Acids on Europium-Substituted Polyoxometalates and the Interaction-Induced Luminescent Enhancement Effect. *ChemPlusChem* **2014,** *79*, 1208-1213.

(97) Zhou, Y.; Zheng, L.; Han, F.; Zhang, G.; Ma, Y.; Yao, J.; Keita, B.; de Oliveira, P.; Nadjo, L., Inhibition of Amyloid-B Protein Fibrillization Upon Interaction with Polyoxometalates Nanoclusters. *Colloids Surf., A* **2011,** *375*, 97-101.

(98) Ly, H. G. T.; Mihaylov, T.; Absillis, G.; Pierloot, K.; Parac-Vogt, T. N., Reactivity of Dimeric Tetrazirconium(IV) Wells–Dawson Polyoxometalate toward Dipeptide Hydrolysis Studied by a Combined Experimental and Density Functional Theory Approach. *Inorg. Chem.* **2015,** *54*, 11477-11492.

(99) Zhang, G.; Keita, B.; Brochon, J.-C.; de Oliveira, P.; Nadjo, L.; Craescu, C. T.; Miron, S., Molecular Interaction and Energy Transfer between Human Serum Albumin and Polyoxometalates. *J. Phys. Chem. B* **2007,** *111*, 1809-1814.

(100) Baroni, S.; Mattu, M.; Vannini, A.; Cipollone, R.; Aime, S.; Ascenzi, P.; Fasano, M., Effect of Ibuprofen and Warfarin on the Allosteric Properties of Haem–Human Serum Albumin. *Eur. J. Biochem.* **2001,** *268*, 6214-6220.

(101) di Masi, A.; Gullotta, F.; Bolli, A.; Fanali, G.; Fasano, M.; Ascenzi, P., Ibuprofen Binding to Secondary Sites Allosterically Modulates the Spectroscopic and Catalytic Properties of Human Serum Heme–Albumin. *FEBS J.* **2011,** *278*, 654-662.

(102) Fasano, M.; Curry, S.; Terreno, E.; Galliano, M.; Fanali, G.; Narciso, P.; Notari, S.; Ascenzi, P., The Extraordinary Ligand Binding Properties of Human Serum Albumin. *IUBMB Life* **2005,** *57*, 787-796.

(103) Sudlow, G.; Birkett, D. J.; Wade, D. N., The Characterization of Two Specific Drug Binding Sites on Human Serum Albumin. *Mol. Pharmacol.* **1975,** *11*, 824-832.

(104) Sudlow, G.; Birkett, D. J.; Wade, D. N., Further Characterization of Specific Drug Binding Sites on Human Serum Albumin. *Mol. Pharmacol.* **1976,** *12*, 1052-1061.

(105) Jiménez-Lozano, P.; Carbó, J. J.; Chaumont, A.; Poblet, J. M.; Rodríguez-Fortea, A.; Wipff, G., Nature of Zr-Monosubstituted Monomeric and Dimeric Polyoxometalates in Water Solution at Different PH Conditions: Static Density Functional Theory Calculations and Dynamic Simulations. *Inorg. Chem.* **2014,** *53*, 778-786.

(106) Jiménez-Lozano, P.; Solé-Daura, A.; Wipff, G.; Poblet, J. M.; Chaumont, A.; Carbó, J. J., Assembly Mechanism of Zr-Containing and Other Tm-Containing Polyoxometalates. *Inorg. Chem.* **2017,** *56*, 4148-4156.

TOC Graphic